International Journal of Steel Structures (2023) 23(2):431–448
https://doi.org/10.1007/s13296-022-00704-0

Online ISSN 2093-6311
Print ISSN 1598-2351

Push-Out Tests on Interlocked Angles Connectors in Steel-Concrete-Steel Composite Structure

Junyi Chen[1,2] · Yonghui Wang[1,2] · Ximei Zhai[1,2] · Xudong Zhi[1,2] · Menghan Sun[3]

Received: 31 July 2022 / Accepted: 4 December 2022 / Published online: 14 December 2022

Abstract
This paper reported a new interlocked angle connector (IAC) for steel-concrete-steel sandwich structures. Shear performances of IACs embedded in normal concrete were studied via a push-out testing program, and the failure mode, shear resistance, and load–slip responses of IACs in normal concrete were obtained. The influences of height, width, thickness, orientation of steel angles, and interlocking bolts on shear behaviours of IACs were experimentally studied. The experimental results indicated that the ultimate shear resistances and slip capacities of IACs were improved via increasing the height, width and thickness of steel angles, while the orientation of steel angles exhibited limited influence on the ultimate shear resistances and failure modes of IACs. In addition, the analytical models were proposed for predicting ultimate shear resistances and load–slip behaviours of IACs. The experimental results were employed to validate the analytical models, and the proposed analytical models were found to provide more accurate predictions on ultimate shear resistances and load–slip behaviours of IACs as compared to the existing design codes.

Keywords Push-out test · Interlocked angles connectors · Shear behaviour · Steel-concrete-steel sandwich structures · Failure mode

1 Introduction

Steel-concrete-steel (SCS) sandwich structure consists of two steel faceplates and a concrete core. Owing to its desirable mechanical performance, SCS sandwich structure has exhibited increasing applications in high-rise buildings (Nie et al., 2013; Yan et al., 2019), shear walls (Qin et al., 2017), immersed tunnels (Lin et al., 2018), shield tunnels (Zhang & Koizumi, 2010), nuclear shielding walls (Varma et al., 2014), ice-resistant walls (Yan et al., 2016), offshore decking (Huang & Liew, 2016; Sohel & Liew, 2014) and protective structures (Remennikov et al., 2019; Wang et al., 2016). Compared with traditional steel structures or reinforced concrete structures, SCS sandwich structures have advantages of good sealing, static (Xie et al., 2007; Yan et al., 2014b, 2020a) and fatigue (Dai & Liew, 2010; Foundoukos et al., 2007) performance, high resistance to blast (Liew & Wang, 2011; Meng et al., 2020; Remennikov et al., 2019) and impact (Sah et al., 2021; Wang et al., 2022b), outstanding seismic performance (Sener et al., 2015; Yan et al., 2019), etc.

The bonding between faceplates and concrete is critical in preventing interfacial separation and slip. Adhesive material or mechanical shear connectors can be employed to transfer shear force and tensile force between concrete and steel faceplates as well as maintain integrity of the SCS sandwich structure. The adhesive materials (e.g., epoxy adhesive) were first adopted for bonding concrete and steel faceplates (Aboobucker et al., 2009; Solomon et al., 1976), and the push-out test was performed with the aim of evaluating its shear strength (Berthet et al., 2011). However, the bonding defects were found to result in separation of steel faceplates from concrete. Previous studies showed that mechanical shear connectors could greatly

✉ Yonghui Wang
wangyonghui@hit.edu.cn

[1] Key Lab of Structures Dynamic Behavior and Control of the Ministry of Education, Harbin Institute of Technology, Harbin 150090, China

[2] Key Lab of Smart Prevention and Mitigation of Civil Engineering Disasters of the Ministry of Industry and Information Technology, Harbin Institute of Technology, Harbin 150090, China

[3] College of Aerospace and Civil Engineering, Harbin Engineering University, Harbin 150000, China

improve ultimate strength and seismic performance of the SCS sandwich structure (Yan et al., 2020b). Therefore, it is necessary to employ mechanical shear connectors for SCS sandwich structures to overcome low bonding strength when using adhesive material.

Headed studs were generally employed as shear connectors for SCS sandwich structures, and desirable bonding behaviours between concrete and steel faceplates could be realized (Pallarés & Hajjar, 2010). Push-out tests were extensively employed to obtain shear behaviours of headed studs (Oduyemi & Wright, 1989; Wang et al., 2022a; Wright et al., 1991), and its ultimate shear resistance was found to be strongly dependent on concrete strength (Wang et al., 2022a). The angle connectors were subsequently applied in the SCS sandwich structure for shield tunnels (Yan et al., 2015). Xie et al. (2004) developed Bi-steel connectors that directly welded to two faceplates. However, the welding apparatus limited the depth of the SCS sandwich structure in a range of 200–700 mm. This restricted their applications in infrastructures, like slim decking. Double J-hook connectors interlocking in pairs were proposed to overcome the limitation on thickness of Bi-steel structures (Liew et al., 2009). In addition, J-hook connectors were also superior to Bi-steel connectors in terms of lower cost and stronger bonding strength. Subsequent experimental studies confirmed that J-hook connectors could effectively bond steel faceplates and concrete (Liew et al., 2009; Yan et al., 2020a). However, the assembly of a large number of J-hook connectors would probably compromise bonding strength (Yan et al., 2020c). Push-out tests were conducted to obtain the shear behaviours of J-hook connectors, and the formulae were proposed for calculating their ultimate shear resistances (Sohel & Liew, 2011; Yan et al., 2014a). Recently, a new enhanced C-channel connector was developed (Wang & Yan, 2020), and its shear behaviour was obtained via conducting push-out tests (Yan et al., 2020b). The enhanced C-channel connector exhibited strong one-direction shear resistance, but weak shear resistance in the perpendicular direction. In addition, drilling holes on steel faceplates resulted in a decrease in the strength of faceplate, and smooth external surfaces of SCS sandwich structures was not able to be realized owing to the presence of bolts. Hence, a new mechanical shear connector, i.e., interlocked angle connector (IAC), was proposed to provide high bonding strength and assure smooth surfaces of SCS sandwich structures. Figure 1 presents the applications of SCS sandwich structures with IACs in nuclear shielding wall and immersed tunnel.

In this study, push-out tests were conducted to obtain shear behaviours of IACs, and the parameters that affect shear behaviours of IACs were also experimentally investigated. Moreover, analytical models were proposed for calculating shear resistances and shear–slip behaviours of IACs.

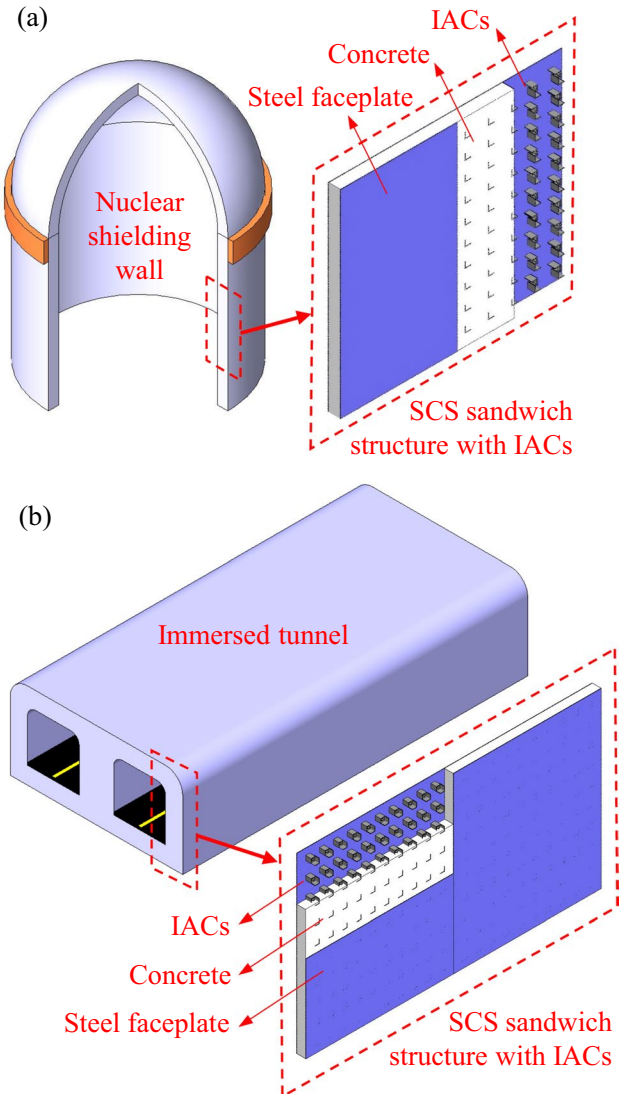

Fig. 1 Application examples of SCS sandwich structure with IACs: (**a**) Nuclear shielding wall and (**b**) Immersed tunnel

2 Test Programme

2.1 Design of Specimens

Figure 2A shows the details of proposed IACs, and a pair of IACs consists of two steel angles, two steel sheets and an interlocking bolt. A pair of steel angles is welded to each inner surface of two faceplates for providing interfacial shear strength between faceplates and concrete. The tensile separation is resisted by the interlocked steel angles. Figures 2b–e illustrate the fabrication procedures of a pair of IACs. Each

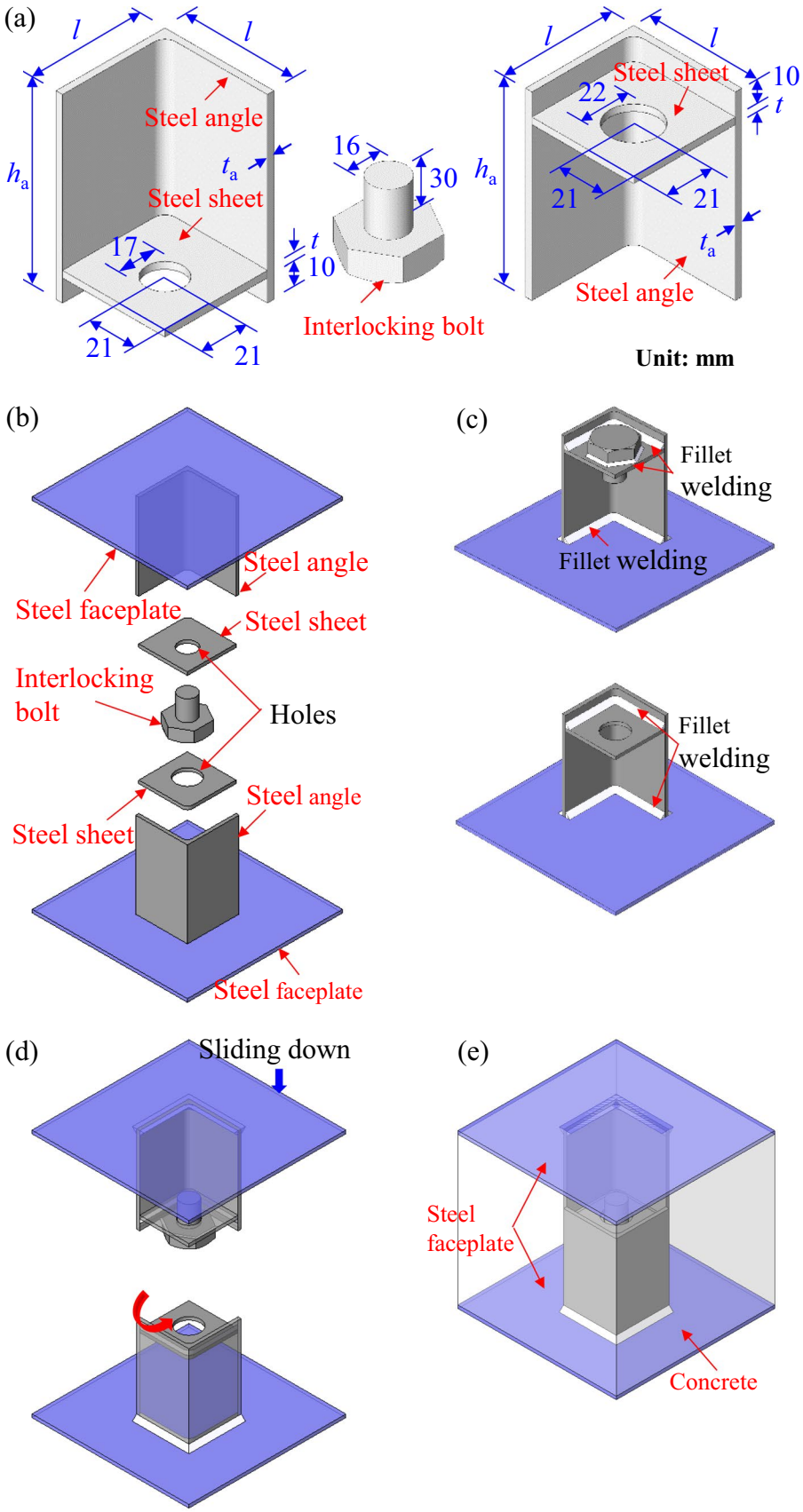

Fig. 2 Fabrication procedures of IACs: (**a**) Dimensions of components of IACs, (**b**) Prefabricating steel angles, steel sheets and interlocking bolts, (**c**) Welding steel angle, steel sheet and interlocking bolt, (**d**) Assembling the steel faceplates, (**e**) Casting concrete

component of the IAC is separately prefabricated first, as shown in Fig. 2b. The steel angle, steel sheet and interlocking bolt are assembled via fillet welding to form the two IACs, as illustrated in Fig. 2c. It should be mentioned that there is no interlocking bolt for the lower IAC. The two IACs are subsequently welded to the two faceplates. The two steel faceplates are assembled via locking the two IACs (see Fig. 2d). Finally, concrete is casted after assembling, as presented in Fig. 2e.

Figure 3a presents the dimensions of specimens fabricated for push-out tests. Reinforcement mesh with $\varphi 8$ HRB400 (diameter is 8 mm and standard value of yield stress is 400 MPa) is embedded in concrete to prohibit splitting of concrete core, as suggested by Xie et al. (2004) and Yan et al. (2014a). The thickness of the steel faceplates is 8 mm, which was found to be able to prevent bending of steel faceplates during loading (Xie et al., 2004). The two steel faceplates measure 410 and 300 mm in length and

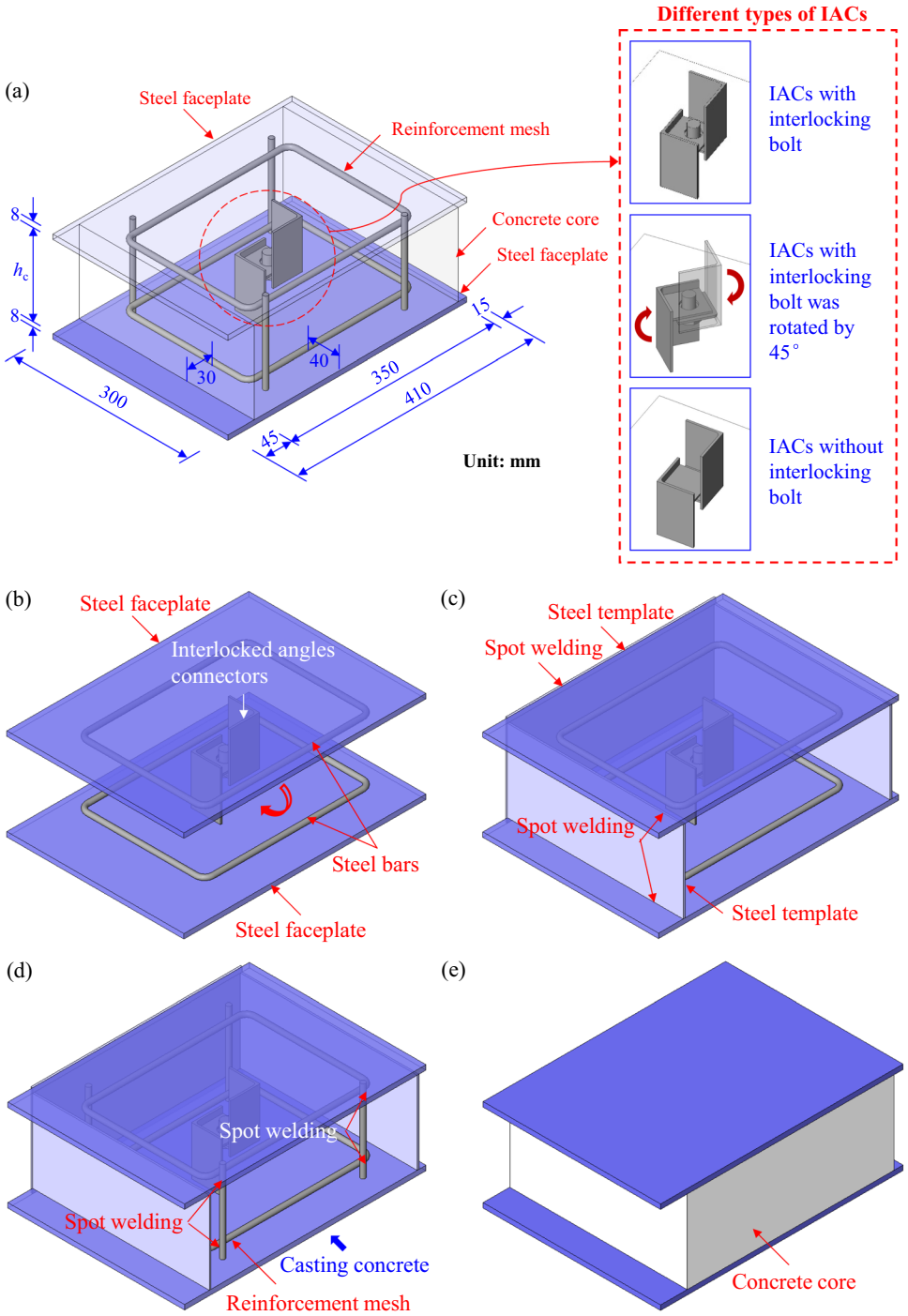

Fig. 3 Fabrication procedures of push-out test specimens: (**a**) Dimensions of push-out test specimens, (**b**) Welding a pair of prefabricated IACs and placing vertical stirrups, (**c**) Fixing the two steel faceplates via two steel templates, (**d**) Welding the steel bars to form the reinforcement mesh, and casting concrete, (**e**) Dismantling steel templates

width, respectively. The concrete core has smaller height than the steel faceplates for allowing slipping between faceplates and concrete core.

There are 24 specimens being initially prepared for the push-out test, among which 23 specimens were successfully tested with valid data being recorded. Table 1 summaries the geometries of the 23 specimens, and the investigated parameters include height of steel angle (h_a), width of steel angles (l), thickness of steel angles (t_a), orientation of steel angles, and presence of interlocking bolts. Specimens A3-1 to A3-8 were designed with different heights (63, 83, 98 and 113 mm) to reveal the effect of h_a on shear behaviours of IACs. Specimens A3-3, A3-4, and A3-9 to A3-12 with different widths (i.e., 50, 45 and 40 mm) were fabricated to obtain the influence of l. Specimens A3-3, A3-4, A4-13 to A5-16 were designed with different thicknesses (i.e., 3.22, 3.82 and 5.00 mm) to study the influence of t_a. Moreover, two specimens (A3-17S and A3-18S) were designed with their IACs being rotated by 45° to investigate the influence of orientation of steel angles, as shown in Fig. 3a. The effect of interlocking bolts on shear behaviours of IACs could be revealed by testing the specimens A3-19E to A5-23E (without interlocking bolts in their IACs).

Figure 3b–e exhibit fabrication procedures of push-out test specimens, which includes (i) welding a pair of prefabricated IACs to two steel faceplates separately (see Fig. 3b), (ii) temporarily fixing two steel faceplates via two steel templates, as shown in Fig. 3c, (iii) welding the steel bars to form the reinforcement mesh, and subsequently casting concrete (see Fig. 3d), and (iv) dismantling steel templates after specimen being cured for more than 28 days, as shown in Fig. 3e.

2.2 Materials

Q235 mild steel was employed for the steel angles, steel sheets and steel faceplates. Three different thicknesses of steel angles and steel sheets were employed for the specimens, and their coupons were cut from each raw material according to GB/T228.1-2010 (MOHURD, 2011). General ready-mixed concrete was employed as the core material of fabricated specimens. The compressive strength of concrete (f_c) was determined as 48.1 MPa via conducting uniaxial compressive loading test on concrete cylinders. The material properties of steel sheets, steel angles and concrete determined from material tests are presented in Table 2.

Table 1 Summary of test specimens

Specimen	t_a (mm)	t (mm)	h_a (mm)	h_c (mm)	l (mm)	r_1 (mm)
A3-1	3.22	2.98	63	100	50	21.0
A3-2	3.22	2.98	63	100	50	21.0
A3-3	3.22	2.98	83	140	50	21.0
A3-4	3.22	2.98	83	140	50	21.0
A3-5	3.22	2.98	98	170	50	21.0
A3-6	3.22	2.98	98	170	50	21.0
A3-7	3.22	2.98	113	200	50	21.0
A3-8	3.22	2.98	113	200	50	21.0
A3-9	3.22	2.98	83	140	45	18.5
A3-10	3.22	2.98	83	140	45	18.5
A3-11	3.22	2.98	83	140	40	16.0
A3-12	3.22	2.98	83	140	40	16.0
A4-13	3.82	3.66	83	140	50	20.5
A4-14	3.82	3.66	83	140	50	20.5
A5-15	5.00	4.92	83	140	50	20.0
A5-16	5.00	4.92	83	140	50	20.0
A3-17S	3.22	2.98	83	140	50	21.0
A3-18S	3.22	2.98	83	140	50	21.0
A3-19E	3.22	2.98	83	140	50	–
A3-20E	3.22	2.98	83	140	50	–
A4-21E	3.82	3.66	83	140	50	–
A5-22E	5.00	4.92	83	140	50	–
A5-23E	5.00	4.92	83	140	50	–

t_a, t–Thicknesses of steel angle and steel sheet, h_a, h_c–Height of steel angle and concrete core, l–Width of steel angle, the geometric parameters of t, h_a, h_c, l, and r_1 are depicted in Figs. 2a and 3a; S denotes the specimen with the steel angles being rotated by 45°; E denotes the specimen without interlocking bolt

Table 2 Material parameters of steel sheet, steel angle and concrete

Steel sheet	E_{ss} (GPa)	f_{sy} (MPa)	f_{su} (MPa)
t = 2.98 mm	204	278	548
t = 3.66 mm	201	288	521
t = 4.92 mm	200	310	536
Steel angle	E_s (GPa)	f_y (MPa)	f_u (MPa)
t_a = 3.22 mm	200	351	629
t_a = 3.82 mm	205	314	570
t_a = 5.00 mm	200	383	673
Concrete	E_c (GPa)	f_c (MPa)	μ
–	24.9	48.1	0.21

E_{ss}, f_{sy}, f_{su}–Elastic modulus, yield stress and ultimate stress of steel sheet; E_s, f_y, f_u–Elastic modulus, yield stress and ultimate stress of steel angle; E_c, f_c, μ–Elastic modulus, compressive strength and Poisson's ratio of concrete

2.3 Test Setup and Instrumentation

Figure 4 depicts the setup and instrumentation of push-out test on IACs. All the specimens were loaded using a 1000-kN loading machine to obtain their shear behaviours. The specimen was placed on a rigid support. A steel block was installed on the top surface of the concrete, and the displacement-controlled actuator was utilized to apply compressive loading to the concrete via the steel block. A load cell was inserted between the steel block and actuator to record the applied load. To measure the interfacial slip between the concrete and steel faceplates, four Linear Variable Differential Transformers (LVDTs) were utilized, with two of them being installed at the top surface of concrete and the rest being installed at the bottom surface. The rate of loading was 0.2 mm/min during the whole test. The signals of LVDTs and load cell were recorded by a data logger, and the sampling rate was 2 Hz.

3 Test Results and Discussions

3.1 Failure Modes

Table 3 summaries the test data and failure modes of 23 specimens. Figure 5a–c exhibit failure modes of representative specimens A3-3, A5-15, A3-17S, respectively. All the specimens experienced shear fracture of IAC along with the evident crushing of concrete near the IAC. Moreover, the specimens with thickest steel angles and steel sheets (A5-15, A5-16, A5-22E and A5-23E) also exhibited splitting of concrete core owing to their higher shear resistances as compared to other specimens.

The observed failure sequences of all tested specimens were similar. Firstly, diagonal cracks of concrete occurred at the tips of steel angles as the concrete near toes of steel angles received local compressive force from steel angles (see Fig. 5a). With further increasing of applied load, the concrete near toe of the steel angle started to be crushed, and diagonal crack continued to develop in its width and length. With the increasing of slip and continuous crushing of concrete, increasing flexural deformation could be observed at the toe of steel angles, which resulted in a gap between concrete and steel angle at the opposite side of crushed concrete. Finally, the specimens lose its load carrying capacity when shear failure occurred to one of the steel angle at its toe.

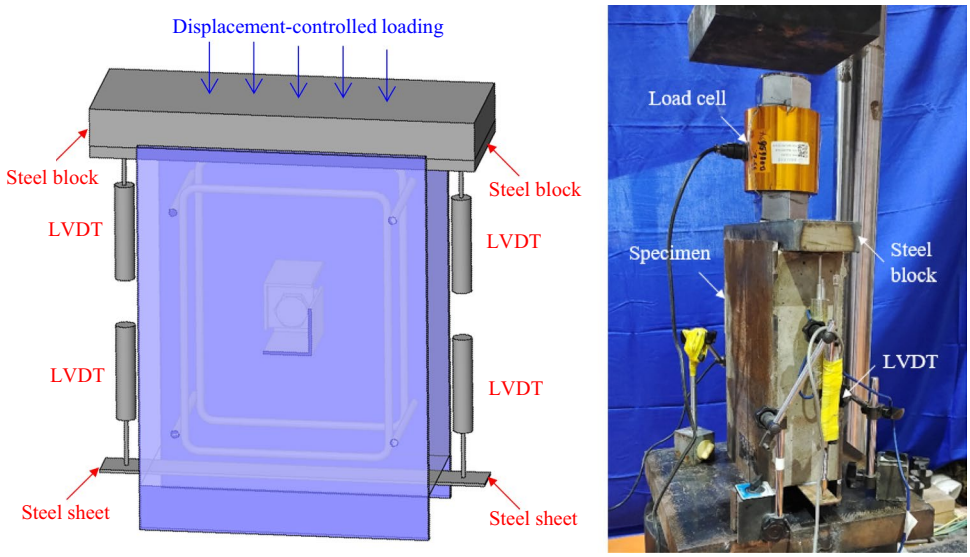

Fig. 4 Push-out test setup and instrumentation

Table 3 Summary of test results

Specimen	P_u (kN)	P_{RK} (kN)	Δ_a (mm)	Δ_u (mm)	K_e (kN/mm)	Failure mode
A3-1	275.99	248.39	6.42	6.95	238	FSC
A3-2	278.57	250.71	4.96	5.86	228	FSC
A3-3	269.74	242.77	6.02	6.69	260	FSC
A3-4	292.37	263.13	5.18	6.57	262	FSC
A3-5	303.22	272.90	5.48	6.47	267	FSC
A3-6	271.77	244.59	4.63	6.35	262	FSC
A3-7	330.48	297.43	4.20	5.65	278	FSC
A3-8	332.30	299.07	4.70	5.40	281	FSC
A3-9	267.23	240.51	3.27	4.62	259	FSC
A3-10	285.61	257.05	5.08	5.34	266	FSC
A3-11	258.25	232.43	3.29	3.82	257	FSC
A3-12	267.46	240.71	5.36	5.87	265	FSC
A4-13	313.20	281.88	4.67	6.46	264	FSC
A4-14	294.80	265.32	5.21	5.76	266	FSC
A5-15	362.50	326.25	6.67	10.62	212	SC
A5-16	371.03	333.93	6.88	9.01	262	SC
A3-17S	281.31	253.18	6.58	8.85	264	FSC
A3-18S	306.20	275.58	6.74	7.96	260	FSC
A3-19E	279.89	251.90	5.81	6.55	259	FSC
A3-20E	294.92	265.43	2.15	4.96	258	FSC
A4-21E	312.62	281.36	6.21	7.67	252	FSC
A5-22E	361.60	325.44	2.89	8.81	270	SC
A5-23E	368.22	331.40	4.98	9.45	263	SC

K_e–Elastic stiffness; the parameters of P_e, P_u, P_{RK}, Δ_e, Δ_a, and Δ_u are depicted in Fig. 7; FSC denotes fracture of shear connectors; SC denotes splitting of concrete

3.2 Load–Slip Curves

The load–slip (P–Δ) curves of all specimens are given in Fig. 6. The generalized P–Δ curve that summarizes the P–Δ curves (i.e., with similar shapes) of all specimens are given in Fig. 7. The generalized P–Δ curve exhibits four stages, including elastic (Stage I), nonlinear developing (Stage II), hardening (Stage III), and recession stages (Stage IV), which is consistent with the observations from Yan et al. (2020b). The elastic stage ends at point A of the generalized P–Δ curve, as shown in Fig. 7. All specimens in this stage exhibit linear relationship between load and slip, and the P–Δ curves of two same specimens are nearly identical. In the nonlinear development stage (curve AB in Fig. 7), the generalized P–Δ curve shows evident nonlinearity owing to the yielding of concrete and steel angles, and meanwhile the stiffness of specimens exhibits significant decrease. In the following hardening stage (curve BC in Fig. 7), the concrete is found to separate from one of the steel faceplates. At point C, the IAC reaches the peak load and subsequently enter recession stage. The load generally exhibits a monotonic decrease in this stage. The concrete at toe of the steel angle is continuously crushed and the steel angle keeps bending, which results in sudden drop of the load (curve DE in Fig. 7). Some of P–Δ curves also exhibit a slight increase in the load, i.e., curve EF in Fig. 7. The load continues to be reduced until the toe of a steel angle is fractured at point G. The P–Δ curves of most specimens exhibit a ductile manner.

3.3 Discussions

3.3.1 Ultimate Shear Resistance, Initial Stiffness, and Slip Capacity

The ultimate shear resistance (P_u) and its corresponding slip (Δ_a) can be directly obtained from the P–Δ curves (see Fig. 7). The initial stiffness (K_e) can be defined as the ratio of P_e to Δ_e, i.e.,

$$K_e = \frac{P_e}{\Delta_e} \tag{1}$$

where P_e is elastic limit shear load which equals to 50% of P_u, as suggested in Eurocode 4 (BSI, 2004), and Δ_e is slip corresponding to P_e.

The slip capacity (Δ_u) is defined as the slip value corresponding to P_{RK} which equals to 90% of P_u following Eurocode 4 (BSI, 2004). Both Δ_u and Δ_a are generally employed

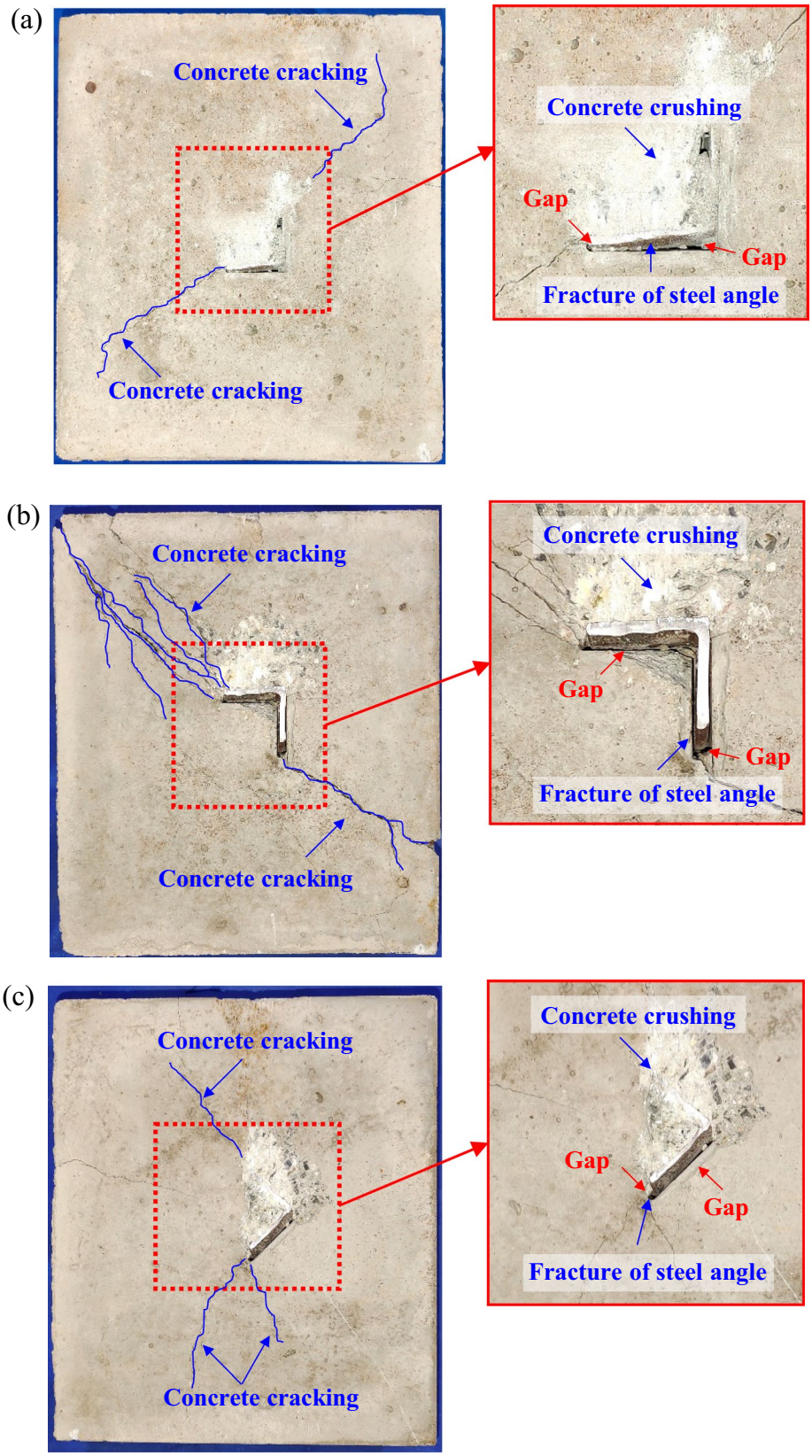

Fig. 5 Failure modes of specimens: (**a**) A3-3, (**b**) A5-15, (**c**) A3-17S

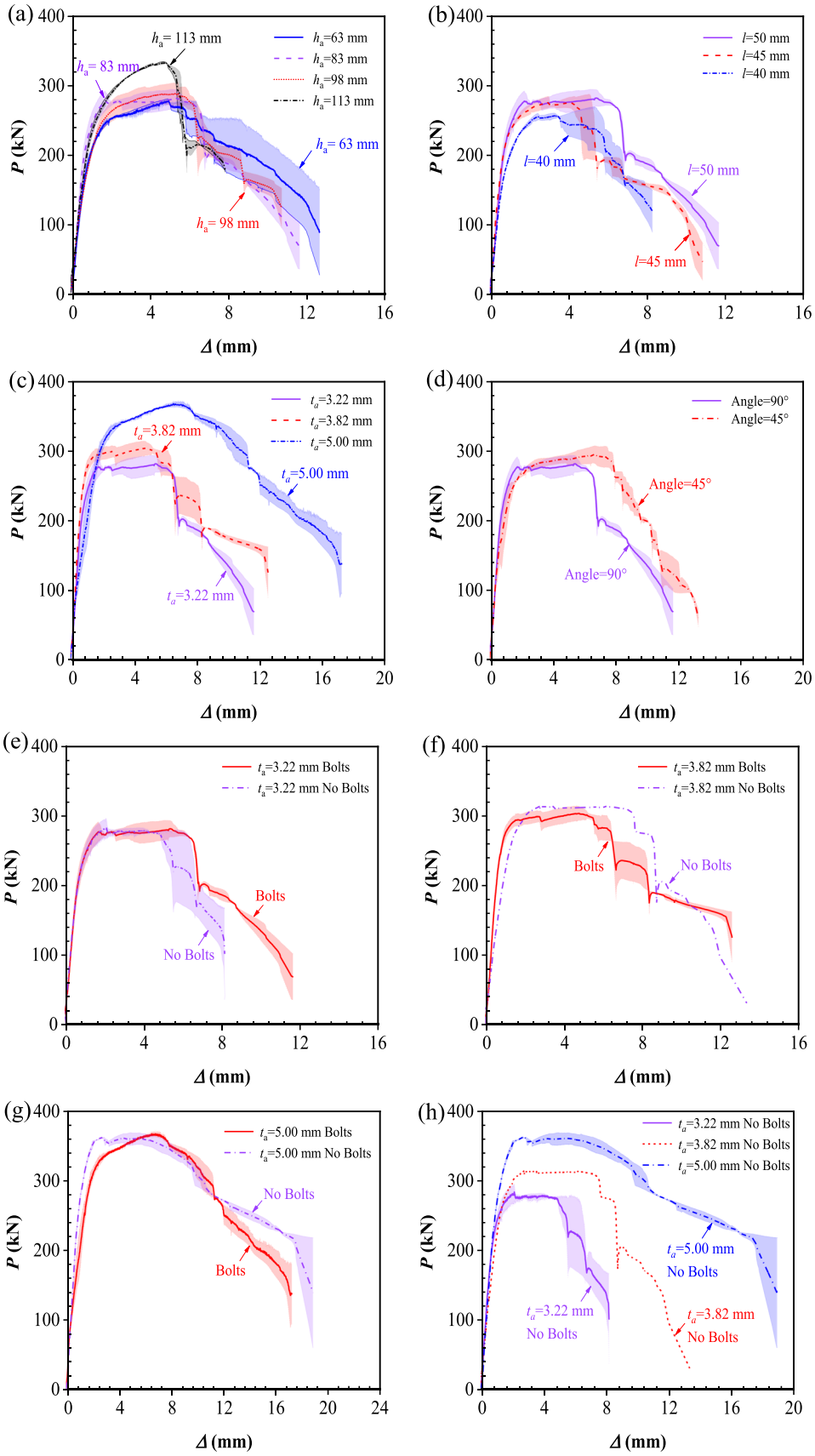

Fig. 6 Influences of different parameters on load–slip behaviours: Effects of (**a**) h_a, (**b**) l, (**c**) t_a, (**d**) orientation of steel angle, (**e**) bolts for specimens with $t_a = 3.22$ mm, (**f**) bolts for specimens with $t_a = 3.82$ mm, (**g**) bolts for specimens with $t_a = 5.00$ mm, (**h**) t_a for specimens without bolts

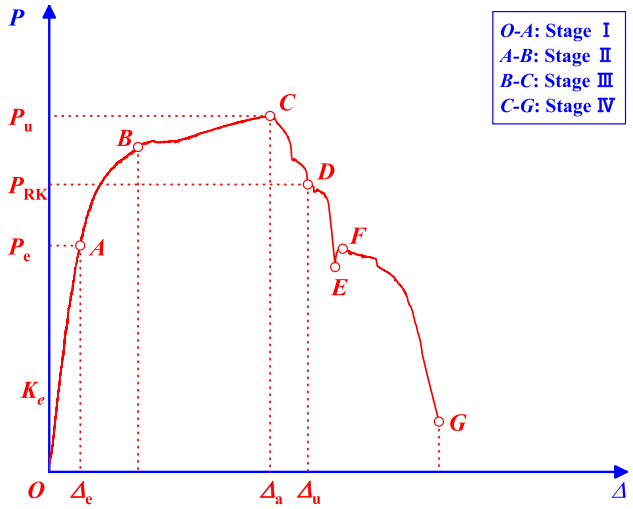

Fig. 7 Generalized load–slip curve

for evaluating the slip capacity of IACs. Table 3 summaries the values of K_e, P_u, Δ_a and Δ_u for all tested specimens.

3.3.2 Effect of Height of Steel Angles (h_a)

The effect of h_a on P–Δ curves is shown in Fig. 6a, and increasing h_a generally results in an improved behaviour of P–Δ curve. As shown in Fig. 8a and b, both P_u and K_e are improved as h_a increases. However, Δ_a and Δ_u exhibit a decreasing trend with the increase of h_a. Larger h_a means thicker concrete core and larger surface area of steel angles embedded into the concrete core, which results in an improvement of P_u. As the interfacial shear force between the concrete core and steel faceplates is transmitted via interaction between steel angles and surrounding concrete, P_u is evidently affected by the surface area of steel angles (or h_a). For the same reason, K_e is also improved with increasing thickness of concrete core (i.e., increasing h_a). Owing to the increased K_e, the values of slip (Δ_a and Δ_u) are generally reduced. When the value of h_a increases from 63 to 83 mm, 98 mm and 113 mm (increased by 31.8, 55.6 and 79.4%), P_u is found to be increased by 1.4, 3.7 and 19.5%, respectively, and the corresponding increments for K_e are 12.0, 13.5 and 20.1%, respectively (Fig. 8a). The increasing percentages of P_u and K_e are significantly less than those of h_a. This is because the interaction magnitude between the concrete core and steel angles exhibits a deceasing trend when it moves away from the toe of steel angle. As the value of h_a is increased from 63 to 83 mm, only slight variations happen to Δ_a and Δ_u. When h_a increases to 98 mm, Δ_a decreases by 11.1%, and the variation of Δ_u is negligible. When h_a increases to 113 mm, Δ_a and Δ_u decrease by 21.8% and 13.9%, respectively (Fig. 8b).

3.3.3 Effect of Width of Steel Angles (l)

The effect of l on P–Δ curves is presented in Fig. 6b, and the load–slip behaviour of IACs is enhanced with increasing l. As shown in Fig. 8c and d, P_u exhibits an increasing trend when the value of l increases. However, limited variation can be found for K_e. In terms of Δ_a and Δ_u, they exhibit an increasing trend with the increase of l. It is noted that increasing l results in a linear increase in cross-section area of steel angles and interaction zone between the concrete and steel angles, which leads to a nearly linear increase of P_u with increasing l, as shown in Fig. 8c. P_u is increased by 5.2% and 6.9%, respectively, as l increases from 40 to 45 mm and 50 mm (increased by 12.5% and 25%). The improvement of P_u is found to be less significant as compared to the increase of l. As the value of l is increased from 40 to 45 mm, both Δ_a and Δ_u exhibit little variation. However, as the value of l is increased from 40 to 50 mm, both Δ_a and Δ_u are significantly increased (i.e., increased by 29.5 and 36.8%, respectively). Test results indicate that increasing width of steel angle (l) can improve both ultimate shear resistance and ductility of IAC owing to the increased cross-section area of steel angles.

3.3.4 Effect of Thickness of Steel Angles (t_a)

Figure 6C presents the effect of t_a on P–Δ curves, and a significant enhancement of load–slip behaviour can be observed with increasing t_a. As shown in Fig. 8e and f, P_u keeps increasing as the value of t_a increases. Meanwhile, K_e initially exhibits increase and subsequently decreases, and both Δ_a and Δ_u exhibit an increasing trend. The larger value of t_a means larger cross-section area and higher flexural stiffness of the steel angle, which results in the improvement of P_u. When t_a is increased by 18.6% and 55.3%, P_u is found to be increased by 8.2 and 30.4%, respectively. It can be observed in Fig. 8e that P_u almost exhibits a linear increase with the increment of t_a, and increasing percentages of P_u are almost half of those of t_a. Hence, increasing thickness of IACs can be an effective way to enhance its ultimate shear resistance. In the case of K_e, it is increased by 0.2% and then decreased by 9.1%, respectively, as t_a is increased from 3.22 mm to 3.82 mm and 5.00 mm. The reduction of K_e (when $t_a = 5.00$ mm) is caused by splitting of concrete, as shown in Fig. 5c. As the value of t_a is increased from 3.22 mm to 3.82 mm, Δ_a and Δ_u decrease by 11.8% and 7.8%, respectively. As the value of t_a is increased from 3.22 mm to 5.00 mm, Δ_a and Δ_u increase by 20.9% and 52.0%, respectively. The evident increase of slip capacity for $t_a = 5.00$ mm is caused by splitting of concrete that results in larger slip. Figure 6h shows that t_a has similar effect on P–Δ curves for IACs without interlocking bolts.

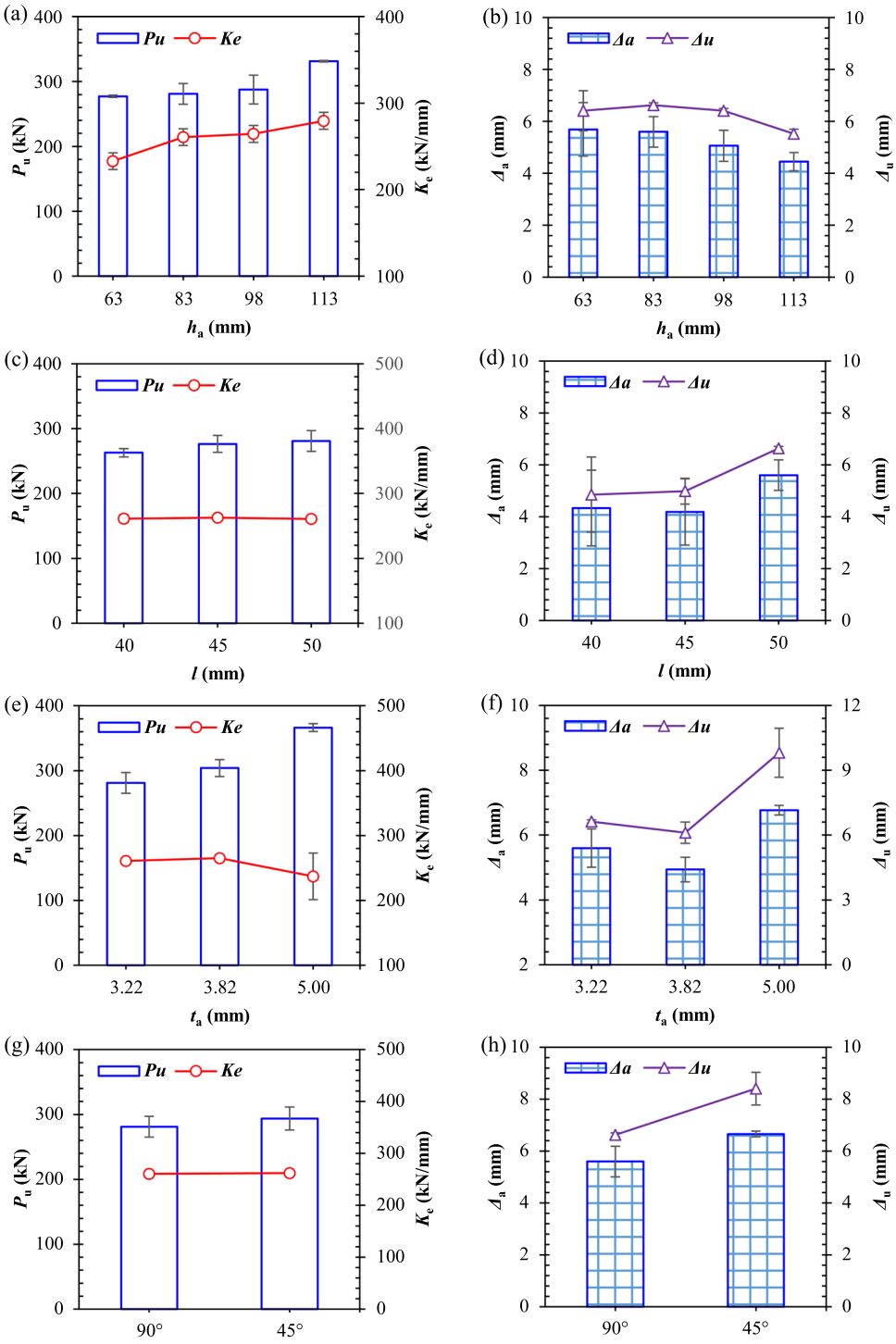

Fig. 8 Influences of different parameters on resistance and slip: Effects of (**a**) h_a on resistance, (**b**) h_a on slip, (**c**) l on resistance, (**d**) l on slip, (**e**) t_a on resistance, (**f**) t_a on slip, (**g**) orientation of steel angle on resistance, (**h**) orientation of steel angle on slip

3.3.5 Effect of Orientation of Steel Angles

Figure 6D shows the effect of orientation of steel angles on P–Δ curves, and only slip capacity (or ductility) is evidently affected by orientation of steel angles. As shown in Fig. 8g and h, P_u and K_e are nearly unchanged (i.e., differences are only 5.0 and 0.4%, respectively) when steel angles are rotated by 45°. However, Δ_a and Δ_u are found to be increased by 15.9 and 26.8%, respectively. The possible reason for the enhancement of slip capacity is that both two webs of steel angles are directly interacted with the concrete during push-out test, which delays the crushing of concrete. The consistent ultimate shear resistance of IACs loaded in different directions promises its applications in SCS sandwich panels or walls whose shear connectors may experience interfacial shear force from any direction.

3.3.6 Effect of Interlocking Bolts on Shear Connectors

Figures 6e–g illustrate the effect of interlocking bolts on *P*–*Δ* curves, the ultimate shear resistance is rarely affected by the presence of interlocking bolts; whereas it exhibits evident influence on the slip capacity (or ductility). As shown in Fig. 9, the variation of P_u and K_e is negligible when comparing specimens with and without interlocking bolts. This is because the interfacial shear force is mainly resisted via the interaction between steel angles and concrete core, which is nearly unaffected by interlocking bolt. In addition to the specimens with $t_a = 3.82$ mm whose slip capacities are enhanced with the presence of interlocking bolts (see Fig. 9d), the slip capacities of specimens with $t_a = 3.22$ mm and 5.00 mm are found to be decreased with presence of interlocking bolts.

4 Analysis on Shear Behaviour of IACs

4.1 Ultimate Shear Resistance

4.1.1 Existing Design Formulae for Steel Angle Connectors

YOKOTA and Kiyomia (1987) proposed a formula for evaluating ultimate shear resistance of the C-shaped angle connector, which is given as:

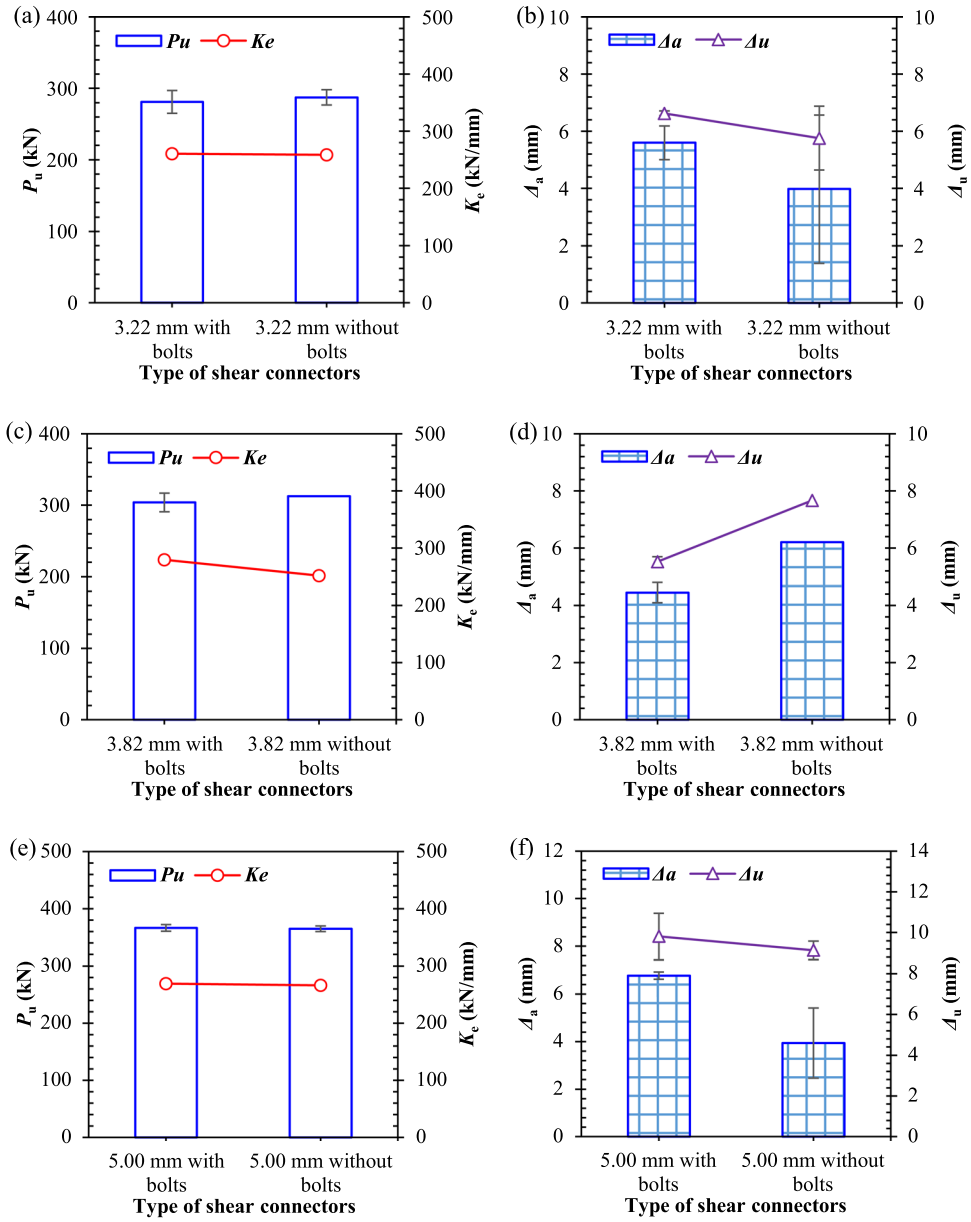

Fig. 9 Influences of interlocking bolts on resistance and slip: Effects of (**a**) bolts for specimens with $t_a = 3.22$ mm on resistance, (**b**) bolts for specimens with $t_a = 3.22$ mm on slip, (**c**) bolts for specimens with $t_a = 3.82$ mm on resistance, (**d**) bolts for specimens with $t_a = 3.82$ mm on slip, (**e**) bolts for specimens with $t_a = 5.00$ mm on resistance, (**f**) bolts for specimens with $t_a = 5.00$ mm on slip

$$P_Y = 88rw\sqrt{t_Y}\sqrt{f_c} \tag{2}$$

where P_Y is nominal strength of an angle connector in (kgf), t_Y is web thickness of angle connector (cm), f_c is compressive strength of concrete (kgf/cm^2), w is length of angle (cm), and r is 1.0 for steel angles.

Khalilian et al. (2015) suggested a formula for predicting shear resistance of C-shaped angle connector, and validated the model with push-out tests. The formula is given as below:

$$P_K = \min\left(4300L^{0.64}t_K^{0.27}f_c^{0.11},\ 0.6F_u t_K L\right) \tag{3}$$

where P_K is shear resistance of angle connector in (N), t_K is web thickness of angle connector (mm), L is length of angle connector (mm), F_u is ultimate strength of steel (MPa), and f_c is compressive strength of concrete (MPa).

Kiyomiya and Yokota (1986) proposed an equation to evaluate shear resistance of angle connectors. The formula is presented as:

$$P_{K\&Y} = 75\sqrt{t_w}L_c\sqrt{f_c} \tag{4}$$

where $P_{K\&Y}$ is shear resistance of angle connector in (lb), t_w is web thickness of connector in (in), L_c is length of connector in (in), and f_c is compressive strength of concrete in (psi).

4.1.2 Proposed Formulae for Shear Resistance of IACs

Equations (2) and (3) were used for C-shaped angle connectors when calculating their shear resistances. In addition, Eq. (4) was developed for angle connectors. There is currently no design guideline available to calculate shear resistance of proposed IACs.

The main parameters that affect shear behaviours of IACs were discussed and presented in Sect. 3. The ultimate shear resistance (P_u) of IAC is evidently affected by h_a, l and t_a; whereas orientation of steel angles and presence of interlocking bolts exhibited limited influence on P_u. GB50017-2017 (MOHURD, 2017) reports that the concrete at toe of shear connectors (e.g., headed stud and steel channel) is subjected to local compression when transmitting interfacial shear force, and therefore the strength and modulus of concrete also affect shear resistance of IACs. The push-out test results in this study also indicate that the interfacial shear force transmitting mechanism of IACs is similar to those of headed studs and steel channels. In addition, it was proved that the ultimate shear resistance of steel angle was significantly influenced by mechanical properties of concrete (Kiyomiya & Yokota, 1986; Yokota & Kiyomia, 1987; AASHTO, 2004; Khorramian et al., 2015; MOHURD, 2017). Shariati et al., (2012, 2013, 2016) studied the ultimate shear resistance of angle connectors with different concrete strengths. The experimental results revealed that the ultimate shear resistance of the angle connector in normal concrete was lower than that in high-strength concrete, which further proved that the ultimate shear resistance of the angle connector was related to the strength and elastic modulus of concrete. Hence, the ultimate shear resistance of IACs is mainly affected by the geometry of steel angle and mechanical properties of concrete.

In this study, multiple regression analysis is performed to establish the relationship between ultimate shear resistance of IACs and its geometrical and material properties. The shear resistance of a single IAC (P_t) is the dependent variable, and h_a, l, t_a, f_c and E_c are considered as independent variables. A general exponential model that contains all the above variables is initially selected, as given below:

$$P_t = \alpha h_a^x t_a^y l^z \sqrt{f_c E_c} \tag{5}$$

where α, x, y and z are coefficients and can be determined by regression analysis.

According to test setup, P_u of a pair of IACs is twice of a single IAC. Hence, P_u can be determined as:

$$P_u = 2P_t \tag{6}$$

Logarithmic transformation was applied to Eq. (5) in order to obtain the equation for linear regression analysis. Four different combinations of coefficients α, x, y and z are considered, among which three models are selected for comparison. Table 4 shows the regression analysis results. The coefficients of variation and correlation for Model 1 are better than the other two models. However, the dimension of the independent variables in this model is not consistent with the dependent variable. Model 2 is the regression analysis model with consistent dimension, as shown in Fig. 10a. Since the fitted values of x, y and z are close to 0.5, 0.5 and 1, respectively, Model 3 is obtained after fixing the aforementioned

Table 4 Results of regression analysis using logarithmic transformations

Model Number	Obtained Exponents				Coefficient of Variation (%)	Coefficient of Correlation
	α	x	y	z		
1	0.0044	0.265	0.506	0.418	0.90	0.84
2	0.196	0.418	0.552	1.030	1.38	0.62
3	0.163	0.500	0.500	1.000	1.42	0.64

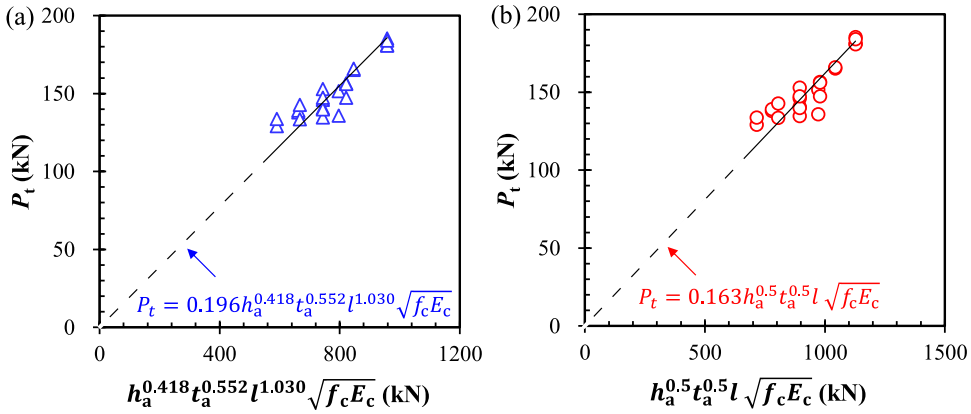

Fig. 10 Regression analysis results for Eq. (5): (a) Model 2, (**b**) Model 3

values of x, y and z, as shown in Fig. 10b. It can be observed from Table 4 that there is no significant difference between Model 2 and Model 3. Considering the consistent dimension of the proposed formula, both Model 2 and Model 3 can be utilized to predict the ultimate shear resistance of IACs.

The ultimate shear resistance of headed stud has an upper limit related to the tensile strength of headed stud, which is $0.8f_uA_s$ (BSI, 2004). Hence, the same upper limit is also employed for the IAC based on the assumption that the shear strength of the weld connection between the steel angle and steel faceplate is greater than that of the steel angle. The formula for calculating P_t is finally given as:

$$P_t = \min\left(0.163h_a^{0.5}t_a^{0.5}l\sqrt{f_cE_c},\ 0.8f_uA_s\right) \quad (7)$$

where f_u and A_s are ultimate tensile strength (MPa) and cross-section area of steel angles (mm^2), respectively.

4.1.3 Verification of Proposed Formulae

The ultimate shear resistances (P_u) of IACs predicted by aforementioned formulae are compared with test data. Figure 11 shows the comparison of test values with predicted values in terms of prediction-to-test ratio. Equation (7) offers the best predictions with an average prediction-to-test ratio to be 1.00, and the standard deviation (SD) and coefficient of variation (COV) of prediction-to-test ratio are found to be 0.014 and 1.42%, respectively. In addition, all the main parameters that affect shear resistance of IACs are considered in the proposed formula. However, the existing design formulae for angle connectors significantly underestimate the shear resistance of IACs. The average prediction-to-test ratio from Eq. (3) is 0.44 with SD of 0.013 and COV of 2.96%. The models predicted by Eq. (2) provide an average prediction-to-test ratio of 0.37 (SD and COV are 0.005 and 1.38%, respectively). It means that Eq. (2) also offers lower predictions on shear resistances of IACs. The lowest predictions are given by Eq. (4) with average prediction-to-test ratio of 0.13 (SD and COV are 0.002 and 1.38%,

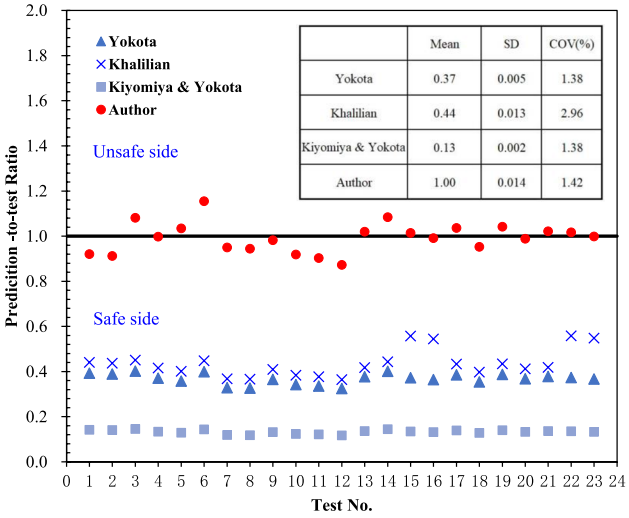

Fig. 11 Scatter of prediction-to-test ratios by different equations

respectively). Hence, considering accuracies of the predictions, Eq. (7) is recommended for predicting the ultimate shear resistance of IACs used in SCS sandwich structures.

Table 5 shows the comparison of ultimate shear resistances of angle connectors between the predictions and tests by Arévalo et al. (2021). The developed empirical formula averagely overestimates the ultimate shear resistances of angle connectors by 10%. The SD and COV of prediction-to-test ratio of the ultimate shear resistance are 0.064 and 5.82%, respectively. This also confirms the accuracy of the proposed empirical formula in predicting the ultimate shear resistances of angle connectors.

4.2 Load–Slip Curves of IACs

According to the test data, nonlinear regression analysis on load–slip curves is performed based on the formulae proposed by Xue et al. (2008), Ollgaard et al. (1971) as well as Gattesco and Giuriani (1996). These load–slip relations are proposed as follows:

Table 5 Validation of developed empirical formula against push-out tests by Arévalo et al. (2021)

Specimen	P_{u_test} (kN)	P_{u_A} by Eq. (7) (kN)	P_{u_A} / P_{u_test}
45–1	137.20	158.39	1.15
45–2	140.55	158.39	1.13
45–3	138.85	158.39	1.14
45–4	154.40	158.39	1.03
45–5	136.00	158.39	1.16
45–6	152.15	158.39	1.04
90–1	161.75	158.39	0.98
90–2	142.15	158.39	1.11
90–3	149.65	158.39	1.06
90–4	148.75	158.39	1.06
90–5	141.55	158.39	1.12
90–6	132.90	158.39	1.19
Mean	–	–	1.10
SD	–	–	0.064
COV(%)	–	–	5.82

P_{u_A} denotes the analytically-predicted ultimate shear resistance of steel angles; P_{u_test} denotes the ultimate shear resistance by test; SD denotes the standard deviation; COV denotes the coefficient of variation

$$\frac{P}{P_u} = \frac{A\Delta}{1 + B\Delta} \tag{8a}$$

$$\frac{P}{P_u} = \left(1 - e^{A\Delta}\right)^B \tag{8b}$$

$$\frac{P}{P_u} = A\sqrt{1 - e^{-B\Delta/A}} + C\Delta \tag{8c}$$

where A, B, and C are coefficients obtained via fitting the experimental data.

The nonlinear regression analysis results of load–slip curves are summarized as follows:

$$\frac{P}{P_u} = \frac{1.62\Delta}{1 + 1.28\Delta} \tag{9a}$$

$$\frac{P}{P_u} = \left(1 - e^{-1.39\Delta}\right)^{1.12} \tag{9b}$$

$$\frac{P}{P_u} = 1.17\sqrt{1 - e^{-0.5\Delta/1.17}} + 0.0048\Delta \tag{9c}$$

Figure 12 presents comparison of load–slip curves between predictions by Eqs. (9a–9c) and test data. It is noted that the load–slip curve predicted by Eq. (9b) exhibits the best fit with experimental results. However, the predictions of load–slip curves based on Eq. (9b) are still not well

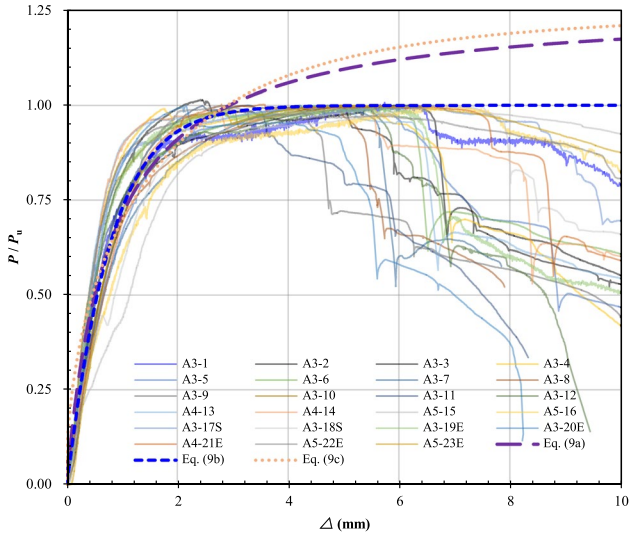

Fig. 12 Experimental and predicted generalized load–slip curves of IACs

matched for all cases. Hence, the quadratic regression analysis that considers the influences of h_a, t_a and l are adopted for the estimation of coefficients A and B in Eq. (8b). The coefficients A and B can be determined as follows:

$$A = a_0 + \sum_{i=1}^{n} a_i x_i + \sum_{i=1}^{n} \sum_{j \geq i}^{n} a_{ij} x_i x_j \tag{10}$$

$$B = b_0 + \sum_{i=1}^{n} b_i x_i + \sum_{i=1}^{n} \sum_{j \geq i}^{n} b_{ij} x_i x_j \tag{11}$$

where n is 3, a_0 and b_0 are constants, a_i, a_{ij}, b_i, b_{ij} ($i, j = 1, 2, 3$) are regression coefficients, x_i and x_j ($i, j = 1, 2, 3$) denote the influenced parameters, i.e., x_1, x_2 and x_3 denote h_a, t_a, l, respectively.

The corresponding coefficients A and B of each tested specimen for Eq. (8b) were obtained by the nonlinear regression analysis. Based on the results of the nonlinear regression analysis, the quadratic regression estimation models of the coefficients A and B for all the specimens are given as follows:

$$A = -0.064333h_a + 0.00099867h_a^2 + 0.074614h_a t_a - 0.0068074h_a l + 0.95603t_a^2 - 0.27476t_a l + 0.0157l^2 \tag{12}$$

$$B = -0.0088297h_a - 0.00041909h_a^2 + 0.029434h_a t_a - 0.00038122h_a l - 0.44586t_a^2 + 0.024516t_a l - 0.00023657l^2 \tag{13}$$

The comparisons of load–slip curves between experiments and predictions are exhibited in Fig. 13. The results

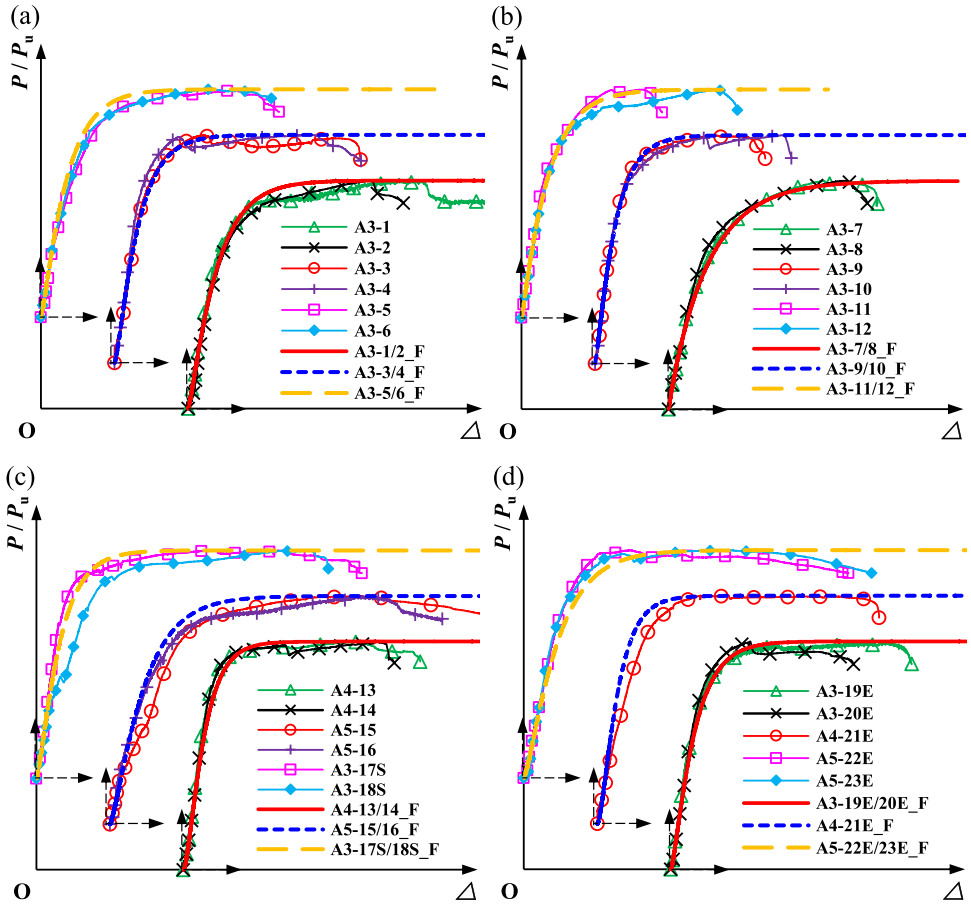

Fig. 13 Comparisons of load–slip curves between experiments and predictions for the specimens: (**a**) A3-1 to A3-6, (**b**) A3-7 to A3-12, (**c**) A4-13 to A3-18S, (**d**) A3-19E to A5-23E

reveal that the predicted load–slip curves are successful in fitting with the load–slip curves of the tests. Thus, Eq. (8b) and Eqs. (12–13) are recommended for predicting the load–slip response of IACs embedded in normal concrete.

5 Conclusions

A novel IAC was developed for SCS sandwich structures, and its shear performance was experimentally and analytically studied. A total of 23 push-out tests were first conducted to obtain failure modes, shear resistances and load–slip behaviours of IACs. Furthermore, analytical models were developed to predict the ultimate shear resistances of IACs. Finally, regression analysis was conducted to yield formulae for predicting load–slip behaviours of IACs. Based on test results and analysis, the following conclusions could be obtained:

(1) The dominate failure mode occurred in the push-out tests on IACs was shear fracture of the steel angle and crushing of concrete. In addition, splitting of concrete was observed for specimens with thicker steel angle and higher shear resistance.

(2) The load–slip (P–Δ) curves of all tested specimens exhibited a similar shape, which could be divided into four stages, i.e., elastic, nonlinear developing, hardening, and recession stage.

(3) The height of steel angles (h_a), width of steel angles (l) and thickness of steel angles (t_a) exhibited significant effects on ultimate shear resistance (P_u) and slip capacity (Δ_u) of IACs. Test results indicated that P_u could be increased by improving h_a, l, and t_a. Moreover, h_a and t_a was found to affect the failure mode of IACs. The orientation of steel angles and presence of interlocking bolts exhibited limited influence on P_u and failure mode of IACs.

(4) The empirical formula for predicting the ultimate shear resistance of IACs was obtained via performing regression analysis of test data, and the SD and COV of prediction-to-test ratio were 0.014 and 1.42%, respectively. Furthermore, a new formula was developed to predict the load–slip behaviour of IACs. The recommended formulae can be employed to facilitate the design of SCS sandwich structures with proposed IACs.

Acknowledgements The research presented in this paper is financially supported by the National Key Research and Development Project of China (Grant No. 2020YFB1901403), the National Natural Science Foundation of China (Grant No. 52278166), the Natural Science Foundation of Heilongjiang Province of China (Grant No. YQ2022E035), the Fundamental Research Funds for the Central Universities (Grant No. HITCE201903 and FRFCU5710051919) and Heilongjiang Postdoctoral Fund (Grant No.: LBH-Q21099 and LBH-TZ1014).

Funding The research presented in this paper is financially supported by the National Key Research and Development Project of China (Grant No. 2020YFB1901403), the National Natural Science Foundation of China (Grant No. 52278166), the Natural Science Foundation of Heilongjiang Province of China (Grant No. YQ2022E035), the Fundamental Research Funds for the Central Universities (Grant No. HITCE201903 and FRFCU5710051919) and Heilongjiang Postdoctoral Fund (Grant No.: LBH-Q21099 and LBH-TZ1014).

Declarations

Conflict of interest All the authors that they have no conflict of interest.

References

AASHTO. (2004). *AASHTO-LRFD bridge design specifications* (3rd ed.). American Association of State Highway and Transportation Officials.

Aboobucker, M. A. M., Wang, T. Y., & Liew, J. Y. R. (2009). An experimental investigation on shear bond strength between steel and fresh cast concrete using epoxy. *The IES Journal Part a: Civil & Structural Engineering, 2*(2), 107–115.

Arévalo, D., Hernández, L., Gómez, C., Velasteguí, G., Guaminga, E., Baquero, R., & Dibujés, R. (2021). Structural performance of steel angle shear connectors with different orientation. *Case Studies in Construction Materials, 14*, e00523.

Berthet, J. F., Yurtdas, I., Delmas, Y., & Li, A. (2011). Evaluation of the adhesion resistance between steel and concrete by push out test. *International Journal of Adhesion and Adhesives, 31*(2), 75–83.

BSI. (2004). *Design of composite steel and concrete structures-Part 1-1: General rules and rules for buildings*. *BS EN 1994-1-1*. Brussels: British Standards Institution.

Dai, X. X., & Liew, J. Y. R. (2010). Fatigue performance of lightweight steel–concrete–steel sandwich systems. *Journal of Constructional Steel Research, 66*(2), 256–276.

Foundoukos, N., Xie, M., & Chapman, J. C. (2007). Fatigue tests on steel–concrete–steel sandwich components and beams. *Journal of Constructional Steel Research, 63*(7), 922–940.

Gattesco, N., & Giuriani, E. (1996). Experimental study on stud shear connectors subjected to cyclic loading. *Journal of Constructional Steel Research, 38*(1), 1–2.

Huang, Z., & Liew, J. Y. R. (2016). Steel-concrete-steel sandwich composite structures subjected to extreme loads. *International Journal of Steel Structure, 16*(4), 1009–1028.

Khalilian, M. (2015). Angle shear connectors capacity. *Modares Civil Engineering Journal, 15*(3), 51–62.

Khorramian, K., Maleki, S., Shariati, M., & Ramli, S. N. H. (2015). Behavior of tilted angle shear connectors. *PLoS ONE, 10*(12), 0144288.

Kiyomiya, O., & Yokota, H. (1986). Strength of shear connector by shape steel in composite member with steel and concrete. In *Proc. of Symposium on Research and Application of Composite Constructions, JSCE* (pp. 113–118).

Liew, J. Y. R., Sohel, K. M. A., & Koh, C. G. (2009). Impact tests on steel–concrete–steel sandwich beams with lightweight concrete core. *Engineering Structures, 31*(9), 2045–2059.

Liew, J. Y. R., & Wang, T. Y. (2011). Novel steel concrete steel sandwich composite plates subject to impact and blast load. *Advances in Structural Engineering, 14*(4), 673–687.

Lin, M., Lin, W., Wang, Q., & Wang, X. (2018). The deployable element, a new closure joint construction method for immersed tunnel. *Tunnelling and Underground Space Technology, 80*, 290–300.

Meng, L., Wang, Y., & Zhai, X. (2020). Modeling and dynamic response of curved steel–concrete–steel sandwich shells under blast loading. *International Journal of Steel Structures, 20*(5), 1663–1681.

MOHURD. (2011). *Metallic materials-tensile testing-part 1: Method of test at room temperature*. *GB/T228. 1–2010*. Beijing: Ministry of Housing and Urban-Rural Development of the People's Republic of China.

MOHURD. (2017). *Standard for design of steel structures. GB50017–2017*. Beijing: Ministry of Housing and Urban-Rural Development of the People's Republic of China.

Nie, J. G., Hu, H. S., Fan, J. S., Tao, M. X., Li, S. Y., & Liu, J. F. (2013). Experimental study on seismic behaviour of high strength concrete filled double-steel-plate composite walls. *Journal of Constructional Steel Research, 88*, 206–219.

Oduyemi, T. O. S., & Wright, H. D. (1989). An experimental investigation into the behaviour of double skin sandwich beams. *Journal of Constructional Steel Research, 19*, 197–220.

Ollgaard, J. G., Slutter, R. G., & Fisher, J. W. (1971). Shear strength of stud connectors in lightweight and normal-weight concrete. *AISC Engineering Journal, 8*(2), 55–64.

Pallarés, L., & Hajjar, J. F. (2010). Headed steel stud anchors in composite structures, Part II: Tension and interaction. *Journal of Constructional Steel Research, 66*(2), 213–228.

Qin, Y., Shu, G. P., Fan, S. G., Lu, Y. J., Cao, S., & Han, H. J. (2017). Strength of double skin steel-concrete composite walls. *International Journal of Steel Structures, 17*(2), 535–541.

Remennikov, A., Gan, E. C. J., Ngo, T., & Netherton, M. D. (2019). The development and ballistic performance of protective steel-concrete composite barriers against hypervelocity impacts by explosively formed projectiles. *Composite Structures, 207*, 625–644.

Sah, T. P., Wang, Y., & Lu, J. (2021). Finite element modeling of steel–concrete–steel sandwich beams with bolt connectors under drop weight impact. *International Journal of Steel Structures, 21*(5), 1878–1893.

Sener, K. C., Varma, A. H., Booth, P. N., & Fujimoto, R. (2015). Seismic behavior of a containment internal structure consisting of composite SC walls. *Nuclear Engineering and Design, 295*, 804–816.

Shariati, M., Ramli, S. N. H., Suhatril, M., Shariati, A., Arabnejad, K. M. M., & Sinaei, H. (2012). Behaviour of C-shaped angle shear connectors under monotonic and fully reversed cyclic loading: An experimental study. *Materials and Design, 41*, 67–73.

Shariati, M., Ramli, S. N. H., Suhatril, M., Shariati, A., Arabnejad, K. M. M., & Sinaei, H. (2013). Comparison of behaviour between channel and angle shear connectors under monotonic and fully reversed cyclic loading. *Construction and Building Materials, 38*, 582–593.

Shariati, M., Ramli, S. N. H., Shariati, A., & Kueh, A. B. H. (2016). Comparative performance of channel and angle shear connectors in high strength concrete composites: An experimental study. *Construction and Building Materials, 120*, 382–392.

Solomon, S. K., Smith, D. W., & Cusens, A. R. (1976). Flexural tests of steel-concrete-steel sandwiches. *Magazine of Concrete Research, 28*(94), 13–20.

Sohel, K. M. A., & Liew, J. Y. R. (2011). Steel–Concrete–Steel sandwich slabs with lightweight core-Static performance. *Engineering Structures, 33*(3), 981–992.

Sohel, K. M. A., & Liew, J. Y. R. (2014). Behavior of steel–concrete–steel sandwich slabs subject to impact load. *Journal of Constructional Steel Research, 100*, 163–175.

Varma, A. H., Malushte, S., Sener, K. C., & Lai, Z. (2014). Steel-plate composite (SC) walls for safety related nuclear facilities: Design for in-plane force and out-of-plane moments. *Nuclear Engineering and Design, 46*(8), 240–249.

Wright, H. D., Oduyemi, T. O. S., & Evans, H. R. (1991). The experimental behavior of double skin composite elements. *Journal of Constructional Steel Research, 19*, 97–110.

Wang, T., & Yan, J. B. (2020). Developments of steel-concrete-steel sandwich composite structures with novel EC connectors. *Journal of Constructional Steel Research, 175*, 106335.

Wang, X., Liu, Y., Chen, A., & Ruan, X. (2022a). Auto-tuning ensemble models for estimating shear resistance of headed studs in concrete. *Journal of Building Engineering, 52*, 104470.

Wang, Y., Zhai, X., Lee, S. C., & Wang, W. (2016). Responses of curved steel-concrete-steel sandwich shells subjected to blast loading. *Thin-Walled Structures, 108*, 185–192.

Wang, Y., Sah, T. P., Liu, S., & Zhai, X. (2022b). Experimental and numerical studies on novel stiffener-enhanced steel-concrete-steel sandwich panels subjected to impact loading. *Journal of Building Engineering, 45*, 103479.

Xie, M., Foundoukos, N., & Chapman, J. C. (2004). Experimental and numerical investigation on the shear behaviour of friction-welded bar–plate connections embedded in concrete. *Journal of Constructional Steel Research, 61*, 625–649.

Xie, M., Foundoukos, N., & Chapman, J. C. (2007). Static tests on steel–concrete–steel sandwich beams. *Journal of Constructional Steel Research, 63*(6), 735–750.

Xue, W. C., Ding, M., Wang, H., & Luo, Z. W. (2008). Static behaviour and theoretical model of stud shear connectors. *Journal of Bridge Engineering, 13*(6), 623–634.

Yan, J. B., Liew, J. Y. R., Sohel, K. M. A., & Zhang, M. H. (2014a). Push out tests on J-hook shear connectors in steel-concrete-steel sandwich structure. *Materials and Structures, 47*(10), 1693–1714.

Yan, J. B., Liew, J. Y. R., Zhang, M. H., & Wang, J. Y. (2014b). Ultimate strength behaviour of steel-concrete-steel sandwich composite structures, Part 1: Experimental and analytical study. *Steel and Composite Structures, 17*(6), 907–927.

Yan, J. B., Liew, J. Y. R., & Zhang, M. H. (2015). Shear-tension interaction strength of J-hook connectors in steel-concrete-steel sandwich structure. *Advanced Steel Construction, 11*(1), 72–93.

Yan, J. B., Liu, X. M., Liew, J. Y. R., Qian, X., & Zhang, M. H. (2016). Steel-concrete-steel sandwich system in Arctic offshore structures: Materials, experiments, and design. *Materials & Design, 91*, 111–121.

Yan, J. B., Yan, Y. Y., Wang, T., & Li, Z. X. (2019). Seismic behaviours of SCS sandwich shear walls using J-hook connectors. *Thin-Walled Structures, 144*, 106308.

Yan, J. B., Guan, H. N., & Wang, T. (2020a). Finite element analysis for flexural behaviours of SCS sandwich beams with novel enhanced C-channel connectors. *Journal of Building Engineering, 31*, 101439.

Yan, J. B., Hu, H., & Wang, T. (2020b). Shear behaviour of novel enhanced C-channel connectors in steel-concrete-steel sandwich composite structures. *Journal of Constructional Steel Research, 166*, 105903.

Yan, J. B., Hu, H., & Wang, T. (2020c). Flexural behaviours of steel-UHPC-steel sandwich beams with J-hook connectors. *Journal of Constructional Steel Research, 169*, 106014.

Yokota, H., & Kiyomia, O. (1987). Load carrying capacity of shear connectors made of shape steel in steel-concrete composite members. Structures division subaqueous tunnels and pipelines laboratory PARI Techinical Note 0595.

Zhang, W., & Koizumi, A. (2010). Behavior of composite segment for shield tunnel. *Tunnelling and Underground Space Technology, 25*(4), 325–332.